The Astrophysical Journal Letters, 946:L2 (10pp), 2023 March 20 https://doi.org/10.3847/2041-8213/acc076

A Binary Origin for the First Isolated Stellar-mass Black Hole Detected with Astrometric Microlensing

Alejandro Vigna-Gómez[1,2] and Enrico Ramirez-Ruiz[3]
[1] Max-Planck-Institut für Astrophysik, Karl-Schwarzschild-Str. 1, D-85748 Garching, Germany; avigna@mpa-garching.mpg.de
[2] Niels Bohr International Academy, Niels Bohr Institute, University of Copenhagen, Blegdamsvej 17, DK-2100, Copenhagen, Denmark
[3] Department of Astronomy and Astrophysics, University of California, Santa Cruz, CA 95064, USA
Received 2022 March 10; revised 2023 February 27; accepted 2023 March 2; published 2023 March 21

Abstract

The Milky Way is believed to host hundreds of millions of quiescent stellar-mass black holes (BHs). In the last decade, some of these objects have been potentially uncovered via gravitational microlensing events. All these detections resulted in a degeneracy between the velocity and the mass of the lens. This degeneracy has been lifted, for the first time, with the recent astrometric microlensing detection of OB110462. However, two independent studies reported very different lens masses for this event. Sahu et al. inferred a lens mass of $7.1 \pm 1.3\,M_{\odot}$, consistent with a BH, while Lam et al. inferred 1.6–4.2 $M_{\odot}$, consistent with either a neutron star or a BH. Here, we study the landscape of isolated BHs formed in the field. In particular, we focus on the mass and center-of-mass speed of four subpopulations: isolated BHs from single-star origin, disrupted BHs of binary-star origin, main-sequence stars with a compact object companion, and double compact object mergers. Our model predicts that most ($\gtrsim$70%) isolated BHs in the Milky Way are of binary origin. However, noninteractions lead to most massive BHs ($\gtrsim$15–20 $M_{\odot}$) being predominantly of single origin. Under the assumption that OB110462 is a free-floating compact object, we conclude that it is more likely to be a BH originally belonging to a binary system. Our results suggest that low-mass BH microlensing events can be useful to understand binary evolution of massive stars in the Milky Way, while high-mass BH lenses can be useful to probe single stellar evolution.

Unified Astronomy Thesaurus concepts: Astrophysical black holes (98); Gravitational microlensing (672); Binary stars (154); Gravitational waves (678)

1. Introduction

Isolated stellar-mass black holes (BHs) are expected to be abundant, with $\approx 10^8$ initially estimated to reside in the Milky Way (Shapiro & Teukolsky 1983). Yet their detection remains elusive. For decades, gravitational microlensing has been the most promising avenue for detecting quiescent stellar-mass compact objects in the Milky Way (e.g., Paczynski 1986, 1996), but because the alignment needed is so accurate and tough to foretell, microlensing is highly infrequent. Given that $\approx 10^8$ BHs are predicted to be drifting through the Milky Way, the probability of seeing a transient brightening of a background star when an isolated BH flits across the field of view (e.g., Wyrzykowski et al. 2016; Wyrzykowski & Mandel 2020) could be high in wide and deep sky surveys.

Several surveys now routinely search for these microlensing events, including the Optical Gravitational Lensing Experiment (OGLE) and the Microlensing Observations in Astrophysics (MOA) survey. These two surveys independently reported (Lam et al. 2022; Sahu et al. 2022) the detection of a compact object using, for the first time, astrometric microlensing of target OGLE-2011-BLG-0462/MOA-2011-BLG-191 (OB110462). However, the reported properties, and particularly the lens mass, were significantly different in each study. Sahu et al. (2022) reported OB110462 as a BH detection with lens mass of $7.1 \pm 1.3\,M_{\odot}$ at a distance of 1.58 ± 0.18 kpc and with transverse space velocity of $\approx 45\,\mathrm{km\,s^{-1}}$. Additionally, Sahu et al. (2022) ruled out a stellar or compact object companion within ≈0.18–230 au. Alternatively, Lam et al. (2022) reported OB110462 as either a neutron star (NS) or a BH with lens mass between 1.6 and 4.2 $M_{\odot}$ at a distance between 0.69 and 1.75 kpc and with transverse motion $<25\,\mathrm{km\,s^{-1}}$. While both studies reported OB110462 as an isolated compact object in the direction of the Galactic bulge, the apparent free-floating nature might not be representative of their origin.

Here, we explore the landscape of compact objects in the context of microlensing targets using binary population synthesis models framed to explain the number density of compact binary mergers as inferred by ground-based gravitational-wave observatories. We focus on the properties of BHs and compact objects belonging to four subpopulations of interest: isolated BHs from a single-star origin, disrupted BHs of binary-star origin, main-sequence stars with a compact object companion, and double compact object mergers. We present the mass and center-of-mass (CoM) speed of BHs and compact binaries following the predictions of rapid population synthesis methods (Section 2). We present these populations generally and place them in the context of isolated BHs (Section 3), particularly OB110462.

2. Binary Population Synthesis

In order to simulate the demographics of BHs in the field we make use of the rapid binary population synthesis element of the COMPAS suite v02.27.05 (Riley et al. 2022). The physical assumptions from this population have been chosen to match predictions of Galactic double NSs (Vigna-Gómez et al. 2018), double compact object mergers (e.g., Neijssel et al. 2019), and Be X-ray binaries in the Small Magellanic Cloud (Vinciguerra et al. 2020).

We simulate 5×10^6 binaries at representative metallicities. These metallicities are the lowest-metallicity models from our stellar evolution tracks ($Z = 0.0001$; Hurley et al. 2000; Riley et al. 2022); a representative metallicity for IZw18 ($Z = 0.0002$; Szécsi et al. 2015); $Z = 0.001$; a representative metallicity for the Small Magellanic Cloud ($Z = 0.0021$; Brott et al. 2011); a representative metallicity for the Large Magellanic Cloud ($Z = 0.0047$; Brott et al. 2011); $Z = 0.01$; a metallicity representative to the Sun ($Z = 0.0142$; Asplund et al. 2009); and a supersolar metallicity $Z = 0.02$. The details of the initial conditions and setup are presented in Table 1 in Appendix A. The data are available (COMPAS 2022).[4]

COMPAS keeps track of the CoM and component speed of the individual binary members and resolves how they are modified when a supernova occurs. To do this, COMPAS follows Appendix B of Pfahl et al. (2002). If a supernova leads to a disruption of the binary, each element speed of the components of the binary is computed. In the case that disruption occurs during the first supernova, the secondary star is followed throughout its remaining lifetime in order to define the stellar remnant and natal kick associated with it. Currently, COMPAS does not follow the evolution of stellar mergers, and therefore they are ignored in this analysis (more information about the implication of stellar mergers in Section 3).

Here, we focus on the mass and CoM speed of systems that are comprised of at least one compact object. Particularly, we center our attention on systems that will lead to BH formation. We distinguish between isolated BHs and compact-object binaries. Isolated BHs can be of single stellar origin (BH_{sin}) or from a binary that becomes disrupted after a supernova (e.g., $BH_{1,2}$, where the subscripts 1 and 2 indicate that the progenitors of the now-disrupted BH were initially the more and less massive star of the binary). Compact-object binaries are those that form when the first supernova leads to NS or BH formation in a bound orbit. For compact-object binaries, we only consider systems with a main-sequence (MS) companion, either NS–MS or BH–MS binaries. These systems are potential progenitors of X-ray binary sources, such as Be X-ray binaries (Reig 2011) or high-mass X-ray binaries (Tauris & van den Heuvel 2006). Finally, we consider double compact object mergers, whether they are BH–NS, BH–BH, or NS–NS binaries. For BH–NS systems, we do not distinguish which compact object formed first. For double compact objects, we only consider those that will merge within a Hubble time via gravitational-wave emission (Peters 1964). We focus on double compact object mergers for two reasons: (i) because they are the systems that will eventually become a single lens and (ii) because they are the systems that will be closer together and more likely to be confused with a single-lens source. For isolated BHs, the mass and speed are those of the remnant after the supernova. For binaries, the mass and speed correspond to the total mass and the CoM speed of the binary.

We classify and count every system from each of the aforementioned subpopulations and estimate their respective yield, which is the number of systems of interest per unit star-forming mass. To estimate the relative contribution of each channel, we need to correct for two things. The first one is to include single stars in our population, which initially assumed 100% binarity. We do so by reusing the primary stars of the widest binaries ($a > 80$ au,[5] where a is the semimajor axis) and using their imparted natal kick, while ignoring the secondary and post-binary evolution (if any). The initial separation distribution is assumed to be a log-uniform distribution, i.e., $p(a) \propto a^{-1}$, and therefore primaries from binaries between $100 \leqslant a/\mathrm{au} \leqslant 1000$ will follow the initial mass function (IMF) and are likely to be noninteracting: i.e., component stars from wide binaries are likely to evolve as two effectively single stars. We also consider a binary fraction, $f_{\rm bin}$, so that $N_{\rm tot} = N_{\rm bin} + N_{\rm sin} = (f_{\rm bin} + f_{\rm sin}) \times N_{\rm tot}$, where $N_{\rm tot}$ is the total number of systems, $N_{\rm bin}$ is the total number of binaries, $N_{\rm sin}$ is the total number of single stars, and $f_{\rm sin}$ is the fraction of single-star systems.[6] We calculate the number of single stars we need to account for following a binary fraction as $N_{\rm sin} = N_{\rm bin}(1 - f_{\rm bin})/f_{\rm bin}$. We use $f_{\rm bin} = 0.8$, which is adequate for stars with initial mass $M > 10\ M_\odot$ (Moe & Di Stefano 2017), which are potential BH progenitors. The second thing we correct for is the total mass of the population. Our simulation includes only stars with mass $M \geqslant 5\ M_\odot$, which follow the Salpeter (1955) IMF. We use the full Kroupa (2001) IMF to account for lower masses, assuming that all low-mass stars are single. With these two corrections, we can quantify the yield per subpopulation of interest as a function of metallicity (Figure 1).

In the simulated population (Figure 1), most isolated BHs ($\approx 8 \times 10^{-4}\ M_\odot^{-1}$) come from the disruption of the primary BH after the first supernova, with similar yields at all metallicities. The yield of single BHs and disrupted secondaries ($\approx 6 \times 10^{-4}\ M_\odot^{-1}$) is similar at high metallicities ($Z \approx 0.02$). However, the yield of single BHs increases at lower metallicities; at $Z \lesssim 0.0002$, they become similar to those of BHs from disrupted primaries. The yield of BH_2, which is comprised of the isolated BHs that originate from the disruption of the secondary, decreases as a function of metallicity ($\approx 4 \times 10^{-4}\ M_\odot^{-1}$ at $Z = 0.0001$). The yield of NS–MS systems ($\approx 2 \times 10^{-4}\ M_\odot^{-1}$) is roughly constant at all metallicities. The yield of BH–MS systems is nonnegligible at low metallicities ($\approx 5 \times 10^{-4}\ M_\odot^{-1}$ at $Z = 0.0001$) and decreases monotonically at high metallicities ($\approx 7 \times 10^{-5}\ M_\odot^{-1}$ at $Z = 0.02$). Merging double compact objects are rare ($< 10^{-4}\ M_\odot^{-1}$ at all simulated metallicities). The decreasing yields as a function of metallicity of BH–MS and BH–BH binaries are correlated with the corresponding increased mass-loss rates via stellar winds at high-metallicity environments (e.g., Neijssel et al. 2019).

After we have identified each subpopulation of interest, we estimate their respective mass and CoM speed probability density function using kernel density estimation (KDE). We calculate an adaptive KDE based on linear diffusion processes as presented in Botev et al. (2010). The kernel for such KDE is assumed to be Gaussian, and the bandwidth parameters are chosen optimally without the need of arbitrary choices or "rules of thumb" (Botev et al. 2010). We use the KDE to define 95% confidence-interval *contours* for each subpopulation (Figure 2).

In Figure 2, we present these contours for the highest metallicity population ($Z = 0.02$). The contours of the populations at other lower metallicities are presented in Figures 3 and 4. The different inferred values from OB110462, as reported by Sahu et al. (2022) and Lam et al. (2022), lead to different

[4] doi:10.5281/zenodo.6346443

[5] This value results in $f_{\rm bin} \approx 0.8$ as specified later in this section.

[6] We assume that higher-multiplicity systems are comprised of an interacting inner binary, such as the ones from our synthetic population.

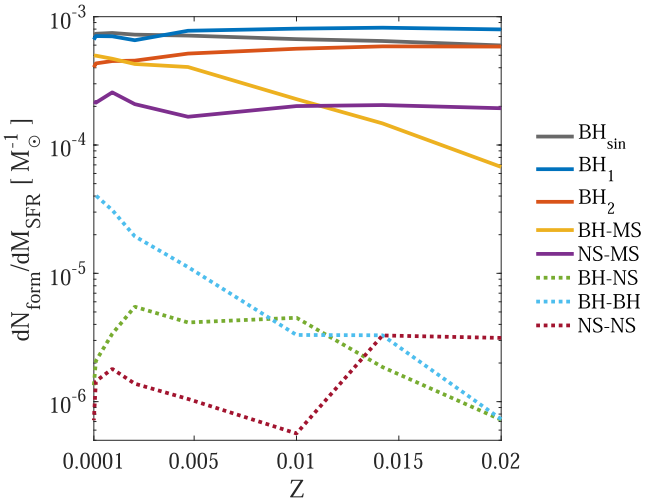

Figure 1. Number of systems of interest per unit star-forming mass. The various yields are calculated based on a population of 5×10^6 massive binaries per metallicity (Section 2). BH_{sin} (solid gray) represents isolated BHs from single-star origin. BH_1 (solid blue) and BH_2 (solid orange) represent disrupted BHs from binary origin; the subscripts 1 and 2 indicate that the progenitor is the initially more and less massive star, respectively. BH–MS (solid yellow) and NS–MS (solid purple) represent bound binaries, comprised of a compact object with a main-sequence companion, just after the first supernova. Double compact objects that will merge within the Hubble time are shown as dotted lines: BH–NS (green), BH–BH (cyan), and NS–NS (burgundy). The color scheme is the same in all figures.

interpretations of the results. The more massive lens mass and higher transverse space velocity values, as reported by Sahu et al. (2022), lie within the contours of the BH_1, BH_2, NS–MS, and BH–NS subpopulations. However, the less massive and lower transverse space velocity values, as reported by Lam et al. (2022), lie only within the contour of the NS–MS subpopulation and marginally within the contour of the binary-origin BH_1, NS–NS, and BH–NS subpopulations. None of the reported values for OB110462 lie within the contour of neither the BH_{sin}, the BH–MS, nor the BH–BH subpopulations.

Finally, we quantify the fraction of BHs from single origin (Figure 5). Approximately 70% of low-mass ($\leqslant 10\,M_\odot$) isolated BHs are from binary origin. In contrast, most high-mass ($>10\,M_\odot$) isolated BHs are from single origin. Moreover, the more massive the BH, the more likely it is to be from single origin (up to ≈80%–90% at some metallicities). If we assume that OB110462 is a BH or a massive ($>1.6\,M_\odot$) NS, it is more likely than it was originated from a binary-star system than from a single star.

3. Discussion

3.1. Summary

We present the landscape of isolated BHs from massive stellar populations in the context of microlensing event OB110462. We did this using the rapid population synthesis element of the COMPAS suite. Our model suggests that OB110462 is an isolated BH of binary origin. We find that, in addition to single and disrupted BHs, bound binaries can be a nonneglibile source of lenses in astronomical populations, both Galactic and extragalactic. We find that most low-mass BHs are from binary origin and most high-mass BHs are from single origin and that there is a distinctive population of such systems that can shed light on the origin of massive binaries and single massive stars in the Milky Way.

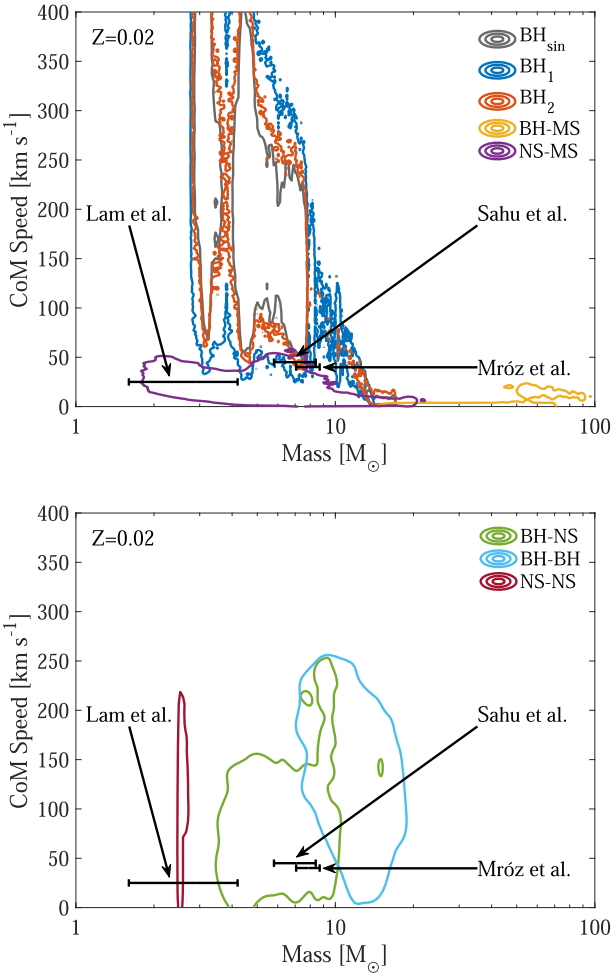

Figure 2. KDE showing the 95% confidence-interval regions for the subpopulation of interest (Figure 1 and Section 2) at $Z = 0.02$. The speed corresponds to the CoM velocity magnitude. The mass corresponds to the BH or total binary mass of the system, depending on whether or not the system is isolated or bound. We show the different reported lens masses of OB110462 as error bars and the transverse space velocity, according to Lam et al. (2022), Sahu et al. (2022), and the more recent analysis from Mróz et al. (2022). The transverse space velocity value from Lam et al. (2022) is an upper limit. Top: subpopulations of isolated BHs (BH_{sin}, BH_1, BH_2) and compact-object binaries (BH–MS, NS–MS). Bottom: subpopulations of double compact object mergers (BH–NS, BH–BH, NS–NS).

3.2. Microlensing Neutron Stars

The fate of stellar remnants depends strongly on their properties at birth. NS remnants are believed to experience a natal kick at formation (e.g., Podsiadlowski et al. 2004). In our COMPAS model, the natal kicks after core-collapse supernovae follow the isolated pulsar velocity distribution (Hobbs et al. 2005). Alternatively, electron-capture supernovae have been predicted to receive low natal kicks (Podsiadlowski et al. 2004) and leave behind an NS with mass $\lesssim 1.3\,M_\odot$ (Nomoto 1984). Therefore, our COMPAS model assumes a bimodal, high-mode ($\sigma = 265$ kms^{-1}) and low-mode ($\sigma = 30$ kms^{-1}) kick distribution (Riley et al. 2022). The low-mode kick is only pertinent for the NS–MS, BH–NS, and NS–NS subpopulations and can only propagate into the isolated BH distribution via mergers of these subpopulations (Section 3.5).

While the low transverse velocity of OB110462 could be associated with low-kick magnitude supernova, modulo the complexity of kinematics, the reported mass ($>1.6\,M_\odot$) is too

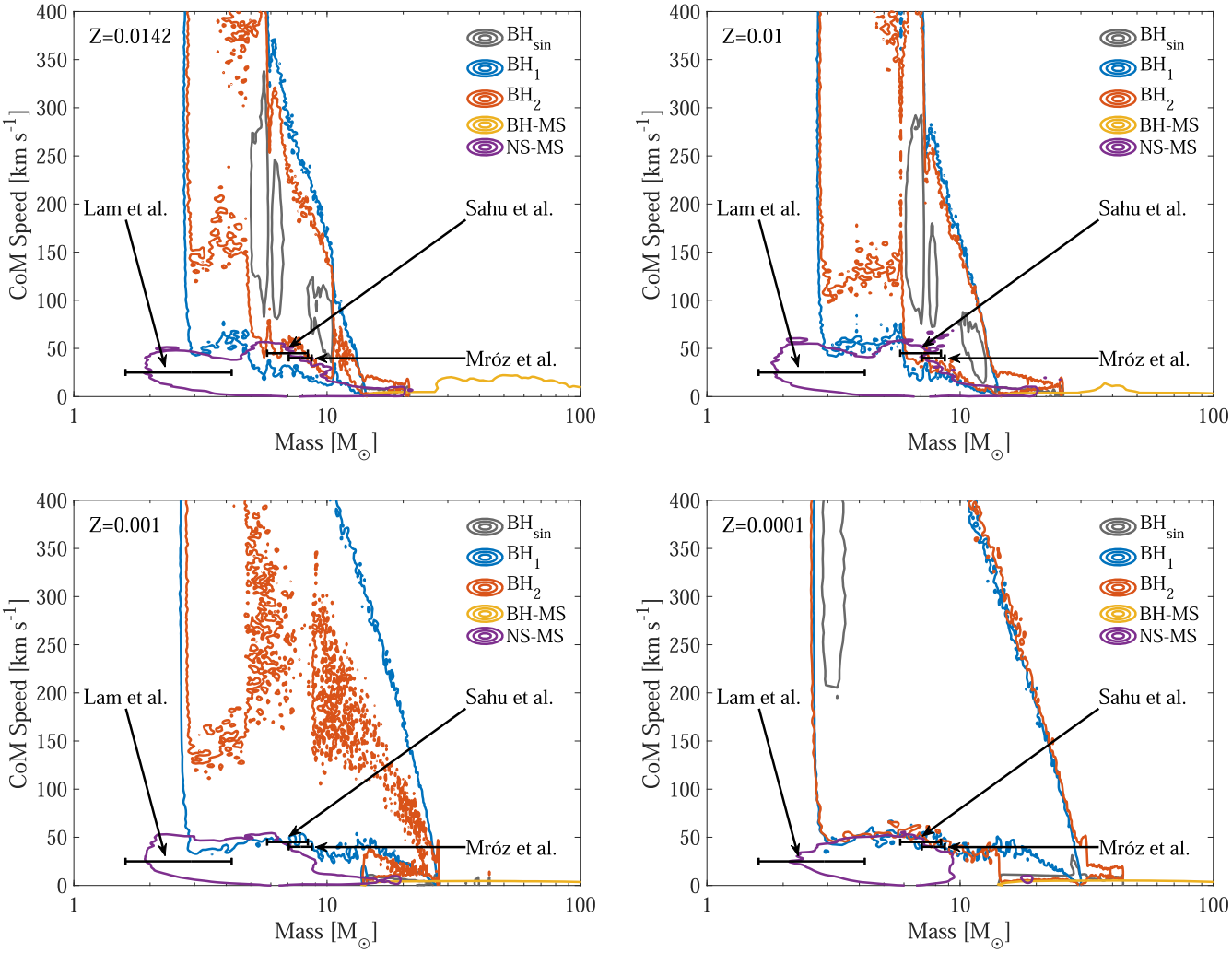

Figure 3. KDE contours showing the 95% confidence-interval regions for the isolated BH and compact binary subpopulations at $Z = \{0.0142, 0.01, 0.001, 0.0001\}$. The bulk of the single BH population at $Z = 0.001$ (bottom left panel) are low speed ($\approx$0 km s^{-1}) and with masses $>10\ M_\odot$ and therefore barely visible in this KDE. For more details, see Section 2 and Figure 2.

heavy (Lam et al. 2022) to be associated with a canonical electron-capture supernova. Lam et al. (2022) reported four events in addition to OB110462, including MB09260. MB09260 is reported with a 0.38:0.44:0.14 probability of being a white dwarf, NS, and BH, respectively. Based solely on the reported (global median) lens mass of 1.37 $M_\odot$, similar to the baryonic mass of the ONeMg core leading to electron-capture supernovae (Nomoto 1984), we consider MB09260 as a more appropriate candidate of an electron-capture supernova (but see Lam et al. 2022 for a discussion on the mass uncertainties). Alternatively, it could also be that the progenitor of MB09260 experienced stripping at some point in its evolution, a process which has been associated with reduced natal kicks (Willcox et al. 2021).

3.3. Microlensing Black Holes

Stars more massive than $\approx$20 $M_\odot$ are thought to be the progenitors of BHs. BH progenitors are more rare and less likely to be single ($f_{\rm sin} < 0.1$ for stars with $M \gtrsim 20\ M_\odot$ according to Moe & Di Stefano 2017). Additionally, the natal kick associated with massive BH remnants is believed to be smaller in magnitude with respect to that of NS progenitors (e.g., Fryer et al. 2012). In COMPAS, the natal kick BHs receive is drawn from the aforementioned high-mode distribution (Section 3.2), but it is usually damped depending on the amount of fallback (Fryer et al. 2012). However, either the (reduced) natal kick or the amount of mass lost during BH formation might lead to a disruption of the binary. The disruption of the binary after the first supernova can lead to a population of low-velocity ($\lesssim$30 kms^{-1}), massive walkaway stars (Renzo et al. 2019), some of which are BH progenitors. Overall, presupernova mass transfer onto a companion will lead to less massive stars at core collapse (e.g., Zapartas et al. 2021) and likely reduced natal kicks. This mass transfer event is also the reason why high-mass BHs are preferentially from single origin: when mass transfer occurs in massive binaries, it can lead to a mass redistribution where the component masses become less massive than the originally more massive star. This mass redistribution depends on the mass of the donor and the accretor and on how conservative the mass transfer episode is (Appendix A). Even for fully conservative mass transfers, most configurations lead to a mass redistribution that results in post-mass-transfer stellar companions less massive than the originally more massive star. For nonconservative mass transfers, this effect is only enhanced. As a summary, for isolated BHs, the binary BH mass distribution is steeper than the single BH mass distribution (Figure 6).

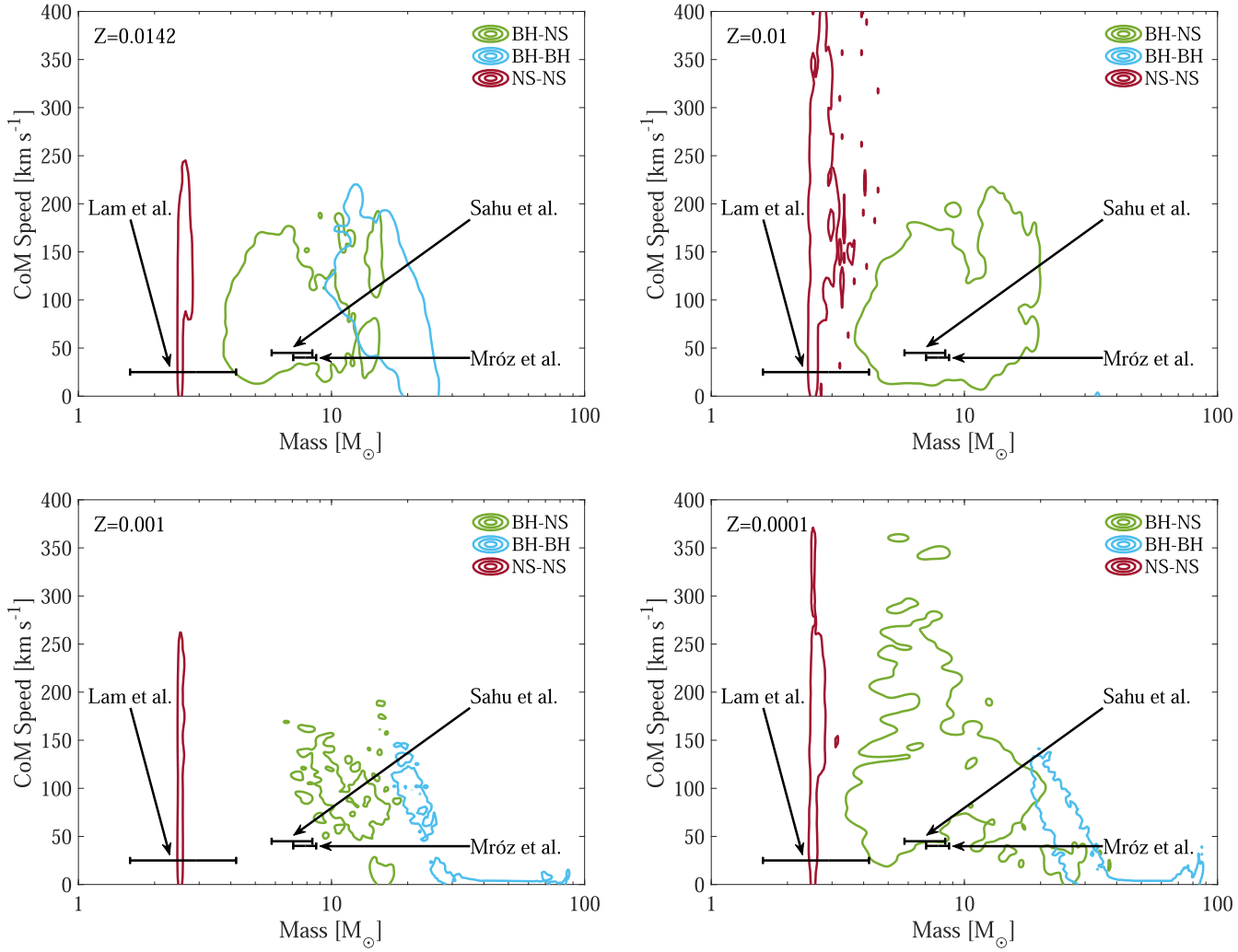

Figure 4. KDE contours showing the 95% confidence-interval regions for double compact object merger subpopulations at $Z = \{0.0142, 0.01, 0.001, 0.0001\}$. The bulk of the BH–BH population at $Z = 0.01$ (top right panel) are low speed ($\approx$0 km s^{-1}) and with masses around $\gtrsim$30 $M_\odot$ and therefore barely visible in this KDE. For more details, see Section 2 and Figure 2.

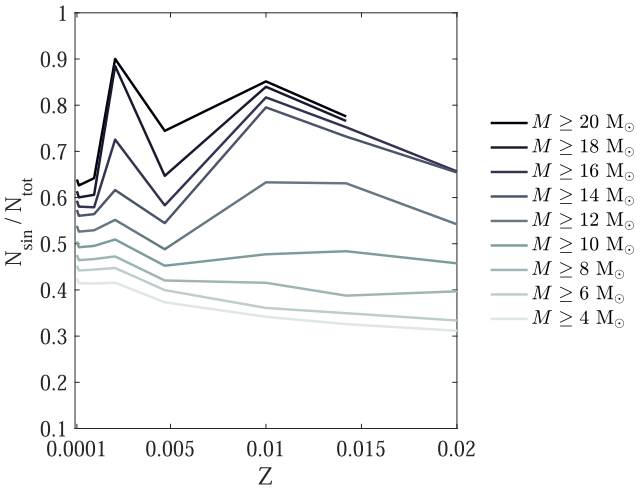

Figure 5. Fraction of isolated BHs of single origin (N_{sin}/N_{tot}), for masses above the threshold mass M, as a function of the simulated metallicities. Isolated high-mass ($\gtrsim$10 $M_\odot$) BHs are predominantly of single-star origin. The darker lines are discontinuous at high metallicities because stellar winds remove enough mass that there are no BHs with mass $\gtrsim$20 $M_\odot$ in our model (Appendix A).

There is an estimated number of $\approx 10^8$–10^9 isolated BHs in the Galaxy (Shapiro & Teukolsky 1983; Timmes et al. 1996). Wiktorowicz et al. (2019) show that the isolated BH population is dominated by isolated BHs of binary origin (also Belczynski et al. 2004; Olejak et al. 2020). Moreover, Wiktorowicz et al. (2019) account for stellar mergers and conclude that the number of isolated BHs from mergers and disrupted binaries is comparable. Our model does not include post-stellar-merger evolution, and therefore we are likely underestimating the amount of isolated BHs of binary origin; however, our model also overestimates the initial binary fraction ($f_{bin} \approx 0.8$) with respect to observations ($f_{bin} \approx 0.7$ according to Sana et al. 2012).

3.4. Surviving Compact Objects in Binary Systems

X-ray binaries are a distinctive population of interacting MS stars with an NS or a BH companion (e.g., Tauris & van den Heuvel 2006; Reig 2011). Our results focus on the moment of the formation of potential X-ray binary progenitors. However, we do not follow the evolution of such systems nor classify those that will emit X-rays and those that will not. Particularly, our total mass

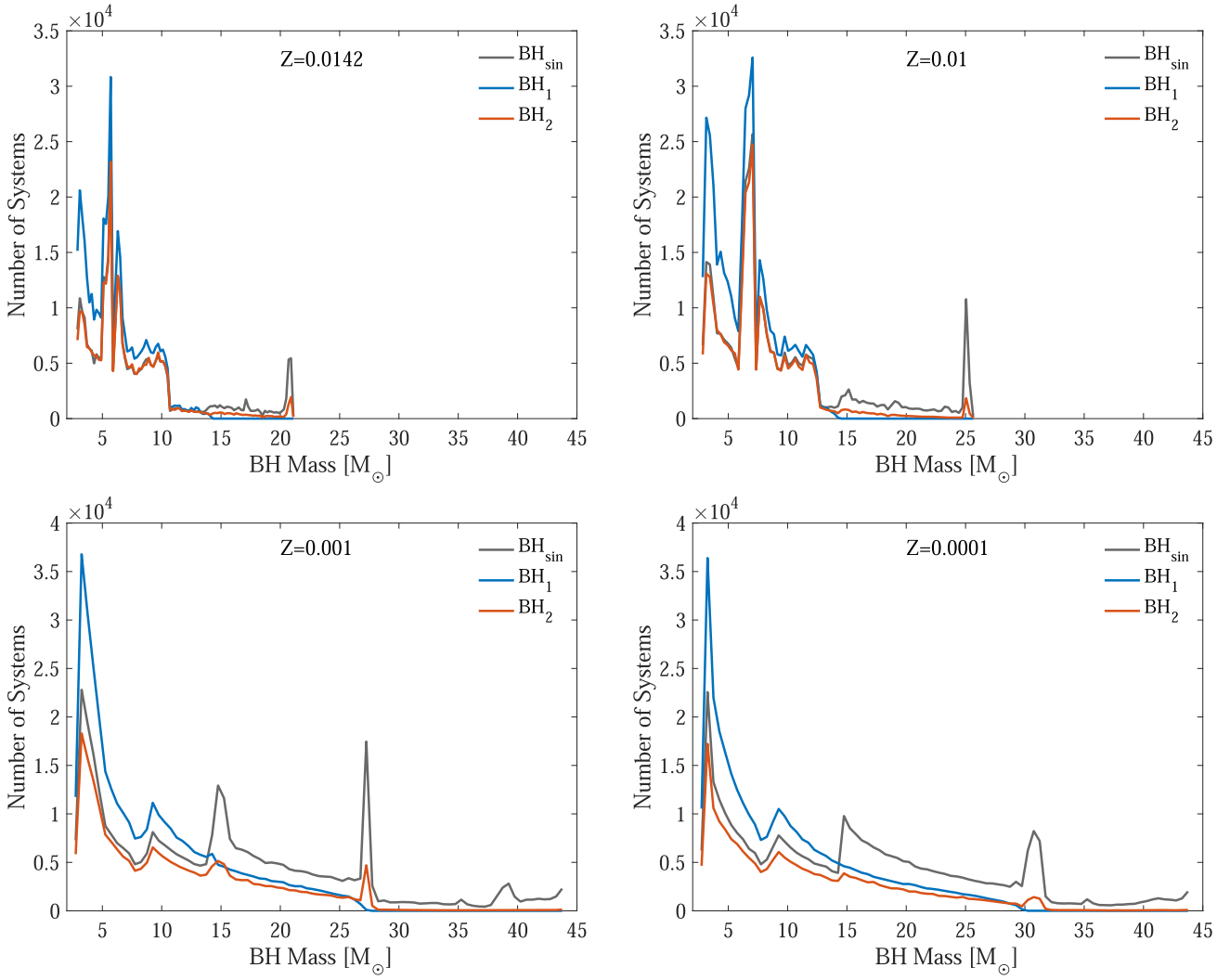

Figure 6. BH mass distribution at $Z = \{0.0142, 0.01, 0.001, 0.0001\}$. The number of isolated BHs from single origin increase as a function of mass for all metallicities. This effect is enhanced at lower metallicities. Low-mass ($\lesssim$10 $M_\odot$) BH lenses can be used to explore binary evolution, while high-mass ($\gtrsim$10 $M_\odot$) BH lenses can be used to understand single stellar evolution (Section 3.6).

estimates are upper limits, as we expect some systems to lose mass via stellar winds and mass transfer episodes. Therefore, while their CoM velocity will not significantly change until the moment of the supernova, the total mass will likely decrease. Some of these binaries will be wide and noninteracting (>100 au; Figure 7) and therefore will not emit X-rays. However, they might be observable with the Gaia mission (Gaia Collaboration et al. 2016) that has been proposed to hunt for BHs (e.g., Breivik et al. 2017; Mashian & Loeb 2017; Yamaguchi et al. 2018; Wiktorowicz & Lu 2020; Andrews 2022; Janssens et al. 2022). Some MS–NS and MS–BH binaries might become giant star binaries (Thompson et al. 2019) and could eventually experience a common-envelope episode (e.g., see Ivanova et al. 2013 for a review), which will further strip the stars, leading them to a close ($\lesssim$0.1 au) orbit configuration. These close, stripped binaries might be difficult to detect (e.g., Götberg et al. 2018) as their luminosity is dependent on their mass and the amount of hydrogen left on their envelope after the stripping episode (e.g., Vigna-Gómez et al. 2022). In the case of OB110462, the presence of any companion more massive than 10% of the identified lens ($\approx$7.1 $M_\odot$) has been excluded within 230 au (Sahu et al. 2022), and there is no evidence for a massive, luminous main-sequence star companion at a larger separation.

3.5. Double Compact Object Binaries

Double compact objects detectable by ground-based gravitational-wave observatories need to be in close ($\lesssim$0.1 au) orbits in order to merge within the age of the universe (Figure 7). In such close orbits, the compact binary can be confused with a single lens (Section 3.9). However, such configurations are extremely rare (Figure 1). A double compact object merger leads to the formation of a single, rotating compact object, most likely a BH. During inspiral, and mostly throughout the merger, mass energy is radiated in the form of gravitational waves, and therefore the post-merger mass is less than the sum of the component BH masses (e.g., Boyle et al. 2008). Moreover, depending on the masses and spins of the component compact objects, the coalescence can lead to a gravitational-wave recoil kick for the post-merger remnant. Nonspinning compact objects, likely representative of the field population (Fuller & Ma 2019) as well as those from the COMPAS simulation, will get a recoil kick in direction of the orbital plane with a magnitude as high as $\approx$175 kms^{-1} (González et al. 2007) and close to $\approx$0 kms^{-1} for either extreme mass ratios or mass ratios close to unity. Therefore, we expect a double compact object merger to decrease the mass and slightly change

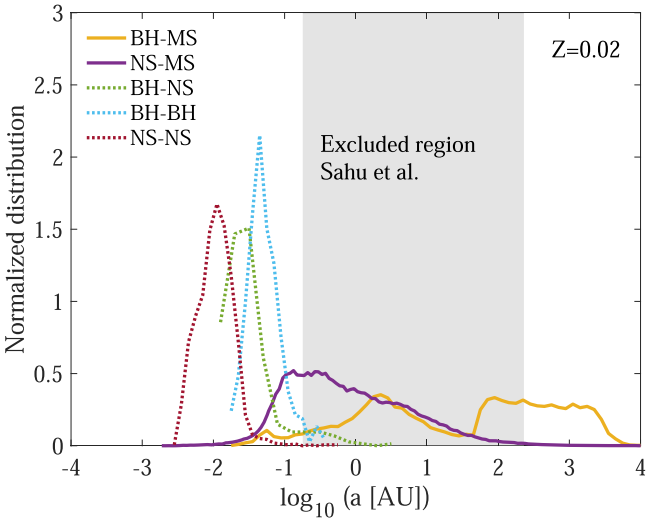

Figure 7. Normalized distributions of the semimajor axis of all binary subpopulations. Compact objects with a main-sequence companion (NS–MS, BH–MS) are shown in solid lines. NS–MS and BH–MS are X-ray binary candidates, particularly if they are in close or eccentric orbits where periastron passage triggers X-ray emitting processes. Double compact object mergers (BH–NS, BH–BH, and NS–NS) are shown in dotted lines. They are in very short periods as we are only considering those that will merge within the Hubble time. The gray shaded region denotes the excluded region of binaries or a companion to the lens mass of OB110462, as derived by Sahu et al. (2022).

the velocity with respect to the contours presented in the bottom panel of Figure 2.

3.6. What We Can Learn from Black Hole Lenses

A population of BH lenses in the Milky Way can be used to explore the physics of massive stars. Lam et al. (2020) performed a single-star single-metallicity population synthesis study, which accounts for selection effects, to suggest that the BH present-day mass function, BH multiplicity, and BH kick velocity distribution can be constrained using the future Nancy Grace Roman Space Telescope microlensing survey (Spergel et al. 2015). That study did not incorporate stellar binaries and therefore is likely to be biased toward a shallower BH present-day mass function.

Shortly after we submitted this manuscript, Andrews & Kalogera (2022) explored how microlensing detections can be used to measure BH natal kicks, particularly in the context of OB110462. Their method relies on backwards integration to trace the origin of compact objects by measuring their peculiar velocity and inferring the natal kick the object received. In contrast, we have forward-modeled a stellar population and calculated the velocities of isolated compact object lenses. These methods are complementary, and we reach a similar conclusion regarding mass-velocity configurations.

Here we have distinguished between a low- and a high- mass population of isolated BH lenses. Low-mass ($\lesssim$10 $M_\odot$) isolated BHs are more likely from binary origin, and therefore the physics of mass transfer, stripping, and orbital dynamics can be probed with these lenses. Additionally, they can be used to explore supernovae, particularly the transition from NS to BH formation and the so-called first BH mass gap (e.g., Wyrzykowski & Mandel 2020 and references therein). High-mass ($\gtrsim$10 $M_\odot$) isolated BHs are more likely from single origin and therefore useful to explore the physics of supernovae (e.g., Fryer et al. 2012), such as fallback (e.g., Vigna-Gómez et al. 2021) and the pair-instability mass gap (e.g., Heger & Woosley 2002; Woosley 2017), as well as stellar winds (e.g., Smith 2014, for a review).

Finally, the predicted mass and velocity distribution of isolated BH lenses depend on the assumptions about the supernova. We explored using an alternative natal kick prescription to gauge the effect on the isolated BH population (Appendix B), which resulted in effectively identical yields but slower CoM speed ($\lesssim$50 km s^{-1}). However, supernova modeling in population synthesis can include variations on the remnant mass prescription or the natal kick distribution, which sometimes can be coupled or dependent on the evolutionary history of the system. Such an exploration is beyond the scope of this work but would be a natural extension in the exploration of stellar-mass BH lenses.

3.7. Systematic Errors

Recently, between the submission of this manuscript and its acceptance, Mróz et al. (2022) analyzed the data as used in Lam et al. (2022) and Sahu et al. (2022) in order to investigate the source of mass discrepancy in OB110462. They infer a lens mass of 7.88 ± 0.82 $M_\odot$ (see e.g., Figure 2), which is in agreement with Sahu et al. (2022). They find that using new photometric OGLE reductions reduces the tension between astrometric and photometric measurements. Moreover, they find that the main source of uncertainty comes from blending from a close, bright neighbor. Finally, they suggest "there is no strong evidence for systematic errors in the HST data reductions by Sahu et al. (2022)" and claim that "Lam et al. (2022) reductions are affected by systematic errors."

3.8. Open Questions

In our population, we consider all binaries to begin their evolution at rest with respect to their environment, and therefore any velocity changes are with respect to this zero-velocity inertial frame of reference. We also assume the dynamical effects associated with supernovae are the only way of disturbing that equilibrium. While massive stars and binaries are believed to be young (<100 Myr) and live their lives in situ, disrupted NSs, BHs, and double compact objects can be as old as the Milky Way (≈10 Gyr). We neglect the origin and long-term evolution of systems in the Galactic potential (e.g., Kelley et al. 2010). While the velocity dispersion of stars in the (thin) disk increases with time, stars are rarely heated above $50 \gtrsim$ km s^{-1} in any direction (e.g., Seabroke & Gilmore 2007). We do not account for systems formed in dense dynamical environments (but see Kıroğlu et al. 2022). However, MS–BH binaries have been detected in globular clusters (Giesers et al. 2018).

Sahu et al. (2022) associated OB110462 with a young object, closer to us than to the Galactic disk; however, they do consider the possibility that it is an older object that is just passing by the location of detection. If OB110462 is a young object formed in the field, particularly in the thin disk, our assumptions are nonetheless reasonable.

3.9. Future Prospects

Conventional gravitational microlensing methods lead to a degeneracy between the mass and the velocity of the lens. Astrometric microlensing lifts this degeneracy by measuring the microlens parallax (e.g., Gould 2000), which led to the more precise mass estimates for OB110462. OB110462 has a

low transverse speed ($\lesssim$45 kms^{-1}) and is in the direction of the Galactic bulge (Lam et al. 2022; Sahu et al. 2022). A lens with a low-magnitude natal kick is more likely to remain within the vicinities of its origin rather than emigrate to the outskirts of the Galaxy; this seems to be the case for OB110462. Finally, we highlight that microlensing events could be comprised of binary lenses (Mao & Paczynski 1991) or binary sources (Jung et al. 2017), both of which lead to a particular type of caustics. These lens-source populations should be investigated in order to determine the most plausible configurations and what we can learn about the observed population.

Although the field is far from being mature, sufficient progress has been made in identifying the most prominent binary configurations leading to microlensing of BHs and NSs. We have thus here endeavored to outline some of the stellar avenues that we believe to be most relevant to interpreting microlensing events arising from BHs and NSs.

We thank Alexey Bobrick, Dan D'Orazio, Stephen Justham, Johan Samsing, and Tom Wagg for useful discussions. We thank the Heising-Simons Foundation and the NSF (AST-1911206, AST-1852393, and AST-1615881) for support. A.V-G. received support through Villum Fonden grant no. 29466.

Software: Scripts used for this study will be made publicly available upon publication in GitHub via https://github.com/avigna/isolated-black-holes.

Appendix A
COMPAS Setup

Our rapid population synthesis simulation is done with COMPAS v02.27.05 (Riley et al. 2022). The details of the initial conditions and setup are presented in Table 1.

Table 1
Initial Values and Default Settings of the Population Synthesis Simulation with COMPAS

Description and Name	Value/Range	Note/Setting
Initial Conditions		
Initial mass $m_{1,i}$	[5, 150] $M_\odot$	Kroupa (2001) IMF $\propto m_{1,i}^{-\alpha}$ with $\alpha_{IMF} = 2.3$ for stars above 5 $M_\odot$
Initial mass ratio $q_i = m_{2,i}/m_{1,i}$	[0.01, 1]	Flat mass ratio distribution $p(q_i) \propto 1$ with $m_{2,i} \geqslant 0.1\ M_\odot$
Initial semimajor axis a_i	[0.01, 1000] au	Flat-in-log distribution $p(a_i) \propto 1/a_i$
Initial metallicity Z_i	[0.0001, 0.03]	Representative metallicities (Section 2)
Initial orbital eccentricity e_i	0	Binaries circular at birth
Fiducial Parameter Settings:		
Stellar winds for hydrogen-rich stars	Belczynski et al. (2010a)	Based on Vink et al. (2000, 2001), including luminous blue variable (LBV) wind mass loss with $f_{LBV} = 1.5$
Stellar winds for hydrogen-poor helium stars	Belczynski et al. (2010b)	Based on Hamann & Koesterke (1998); Vink & de Koter (2005)
Max transfer stability criteria	ζ-prescription	Based on Vigna-Gómez et al. (2018) and references therein
Mass transfer accretion rate	thermal timescale	For stars: Vigna-Gómez et al. (2018); Vinciguerra et al. (2020)
	Eddington-limited	For compact objects
Nonconservative mass loss	isotropic re-emission	Massevitch & Yungelson (1975); Bhattacharya & van den Heuvel (1991); Soberman et al. (1997)
		Tauris & van den Heuvel (2006)
Case BB mass transfer stability	always stable	Based on Tauris et al. (2015); Tauris et al. (2017); Vigna-Gómez et al. (2018)
CE prescription	$\alpha - \lambda$	Based on Webbink (1984); de Kool (1990)
CE efficiency α-parameter	1.0	
CE λ-parameter	$\lambda_{Nanjing}$	Based on Xu & Li (2010a, 2020b) and Dominik et al. (2012)
Hertzsprung gap (HG) donor in CE	pessimistic	Defined in Dominik et al. (2012): HG donors do not survive a CE phase
SN natal kick magnitude v_k	[0, ∞) km s^{-1}	Drawn from a Maxwellian distribution with a user-defined standard deviation (σ_{rms}^{1D})
SN natal kick polar angle θ_k	[0, π]	$p(\theta_k) = \sin(\theta_k)/2$
SN natal kick azimuthal angle ϕ_k	[0, 2π]	Uniform $p(\phi) = 1/(2\pi)$
SN mean anomaly of the orbit	[0, 2π]	Uniformly distributed
Core-collapse SN remnant mass prescription	delayed	From Fryer et al. (2012), which has no lower BH mass gap
USSN remnant mass prescription	delayed	From Fryer et al. (2012)
ECSN remnant mass prescription	$m_f = 1.26\ M_\odot$	Baryonic to gravitational mass relation using the equation of state from Timmes et al. (1996)
Core-collapse SN velocity dispersion σ_{rms}^{1D}	265 km s^{-1}	1D rms value based on Hobbs et al. (2005)
USSN and ECSN velocity dispersion σ_{rms}^{1D}	30 km s^{-1}	1D rms value based on e.g., Pfahl et al. (2002); Podsiadlowski et al. (2004)
PISN/PPISN remnant mass prescription	Marchant et al. (2019)	As implemented in Stevenson et al. (2019)
Maximum NS mass	$max_{NS} = 2.5\ M_\odot$	Following Fryer et al. (2012)
Tides and rotation		Not included
Simulation Settings		
Total number of binaries sampled per metallicity	5×10^6	
Sampling method	Monte Carlo	
Binary fraction	$f_{bin} = 1$	
Binary population synthesis code	COMPAS	Riley et al. (2022)

Appendix B
Alternative Natal-kick Distribution

An understanding of the physics of supernovae is an ongoing endeavor (see, e.g., Burrows & Vartanyan 2021 for a recent review). In the context of binary population synthesis, supernova physics is one of the major uncertainties and is often parameterized in order to explore their impact in rates and distributions of, e.g., electromagnetic transients and gravitational-wave sources. In rapid population synthesis, the details of supernovae cannot be incorporated, and therefore supernovae are simplified to instantaneous events where the mass, type, and natal kick of the remnant are determined by the structure of the progenitor. For example, the supernova prescription used in the COMPAS default model (Fryer et al. 2012; see also Appendix A) determines the compact-object remnant given the presupernova mass of the carbon-oxygen core and envelope (if any) of the stellar progenitor. Fryer et al. (2012) account for mass fallback to the newly born compact object, which results in two effects: increasing the mass and damping the natal kick of the compact-object remnant. For BH formation, the natal kick distribution is damped with respect to the Hobbs et al. (2005) velocity dispersion (Appendix A); for the most massive ($\gtrsim$10 $M_\odot$) stellar-mass BHs, complete fallback results in no natal kick.

We explore the effect of an alternative natal kick distribution in our population. We follow the natal kick formula from Bray & Eldridge (2016), where the kick velocity $v_{\rm kick} = \alpha(M_{\rm ejecta}/M_{\rm remnant}) + \beta$, with $\alpha = 100$ and $\beta = -170$ (Bray & Eldridge 2018), scales linearly with the ejecta mass. This formula was originally introduced and studied in the context of young NS populations (Bray & Eldridge 2016) but has since been used in the context of isolated BHs and microlensing events (e.g., Wiktorowicz 2019; Wiktorowicz & Lu 2020). We choose this as an alternative model for the clear physical meaning, the simplicity of the implementation, and because the natal kick is decoupled from the remnant mass prescription, which allows us to compare exclusively the effect of the natal kick with the resulting population.

We create an identical population to our default model, at $Z = 0.02$, with the only difference that we obtain the natal kick from the aforementioned model (Bray & Eldridge 2016, 2018) instead of sampling it from a (default) Maxwellian distribution (Hobbs et al. 2005). First, we explore how the yields of the subpopulations of interest are affected by this alternative natal kick distribution. For the isolated BH population, the yields are effectively identical to those from our default model. For the BH–MS and NS–MS populations, the yields increase at most by a factor of a few with respect to our default model. However, for the double compact object populations, the yields from the alternative model can be up to 1 order of magnitude larger than for our default model; however, these rates are still at least 1 order of magnitude less than those from isolated BHs. Figure 8 shows the subpopulations of interest in the mass versus CoM speed parameter space (see Figure 2). The effect of the alternative natal kick distribution is mostly noticeable in the isolated BH population. While the mass range of isolated BHs remains similar with respect to the default model, the CoM is decreased drastically ($\lesssim$50 km s^{-1}); however, the subpopulations of isolated BHs (BH_{sin}, BH_1, and BH_2) are still consistent with one another, occupying the same parameter space. This is a consequence of more massive BHs having less ejecta, resulting in low kicks (for complete fallback, the formula from Bray & Eldridge (2016, 2018) can result in negative kick magnitudes, which we cap to 0). This model favors a low speed isolated BH population. For the BH–MS and NS–MS populations, the alternative natal kick model widens both the mass and CoM speed distributions but only slightly. Finally, the mass and CoM speed distributions of double compact objects are similar in both natal kick models.

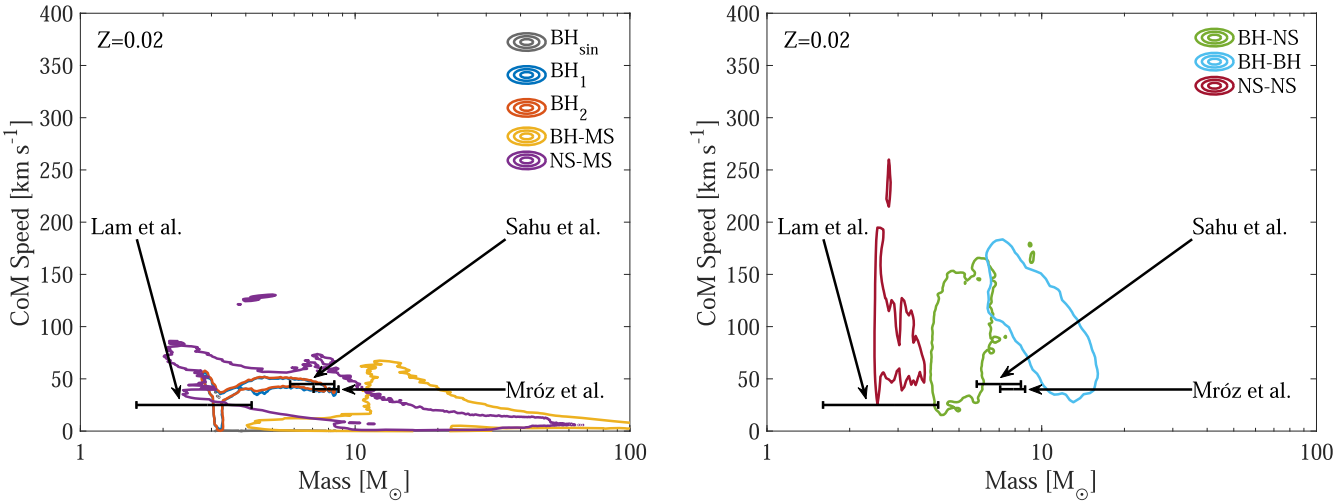

Figure 8. Results using the (alternative) natal kick model from Bray & Eldridge (2016). Besides the natal kick distribution, all other assumptions are identical to the default model (Appendix A). Additionally, the layout here is identical to that of Figure 2, which allows for a direct comparison (more details in Appendix B).

ORCID iDs

Alejandro Vigna-Gómez https://orcid.org/0000-0003-1817-3586
Enrico Ramirez-Ruiz https://orcid.org/0000-0003-2558-3102

References

Andrews, J. J. 2023, ApJ, 944, 146
Andrews, J. J., & Kalogera, V. 2022, ApJ, 930, 159
Asplund, M., Grevesse, N., Sauval, A. J., & Scott, P. 2009, ARA&A, 47, 481
Belczynski, K., Bulik, T., Fryer, C. L., et al. 2010a, ApJ, 714, 1217
Belczynski, K., Dominik, M., Bulik, T., et al. 2010b, ApJL, 715, L138
Belczynski, K., Sadowski, A., & Rasio, F. A. 2004, ApJ, 611, 1068
Bhattacharya, D., & van den Heuvel, E. P. J. 1991, PhR, 203, 1
Botev, Z. I., Grotowski, J. F., & Kroese, D. P. 2010, AnSta, 38, 2916
Boyle, L., Kesden, M., & Nissanke, S. 2008, PhRvL, 100, 151101
Bray, J. C., & Eldridge, J. J. 2016, MNRAS, 461, 3747
Bray, J. C., & Eldridge, J. J. 2018, MNRAS, 480, 5657
Breivik, K., Chatterjee, S., & Larson, S. L. 2017, ApJL, 850, L13
Brott, I., de Mink, S. E., Cantiello, M., et al. 2011, A&A, 530, A115
Burrows, A., & Vartanyan, D. 2021, Natur, 589, 29
COMPAS, T. 2022, COMPAS v02.27.05 output at representative metallicities, doi:10.5281/zenodo.6346444
de Kool, M. 1990, ApJ, 358, 189
Dominik, M., Belczynski, K., Fryer, C., et al. 2012, ApJ, 759, 52
Fryer, C. L., Belczynski, K., Wiktorowicz, G., et al. 2012, ApJ, 749, 91
Fuller, J., & Ma, L. 2019, ApJL, 881, L1
Gaia Collaboration, Prusti, T., de Bruijne, J. H. J., et al. 2016, A&A, 595, A1
Giesers, B., Dreizler, S., Husser, T.-O., et al. 2018, MNRAS, 475, L15
González, J. A., Sperhake, U., Brügmann, B., Hannam, M., & Husa, S. 2007, PhRvL, 98, 091101
Götberg, Y., de Mink, S. E., Groh, J. H., et al. 2018, A&A, 615, A78
Gould, A. 2000, ApJ, 542, 785
Hamann, W. R., & Koesterke, L. 1998, A&A, 335, 1003
Heger, A., & Woosley, S. E. 2002, ApJ, 567, 532
Hobbs, G., Lorimer, D. R., Lyne, A. G., & Kramer, M. 2005, MNRAS, 360, 974
Hurley, J. R., Pols, O. R., & Tout, C. A. 2000, MNRAS, 315, 543
Ivanova, N., Justham, S., Chen, X., et al. 2013, A&ARv, 21, 59
Janssens, S., Shenar, T., Sana, H., et al. 2022, A&A, 658, A129
Jung, Y. K., Udalski, A., Yee, J. C., et al. 2017, AJ, 153, 129
Kelley, L. Z., Ramirez-Ruiz, E., Zemp, M., Diemand, J., & Mandel, I. 2010, ApJL, 725, L91
Kıroğlu, F., Weatherford, N. C., Kremer, K., et al. 2022, ApJ, 928, 181
Kroupa, P. 2001, MNRAS, 322, 231
Lam, C. Y., Lu, J. R., Hosek, M. W. J., Dawson, W. A., & Golovich, N. R. 2020, ApJ, 889, 31
Lam, C. Y., Lu, J. R., Udalski, A., et al. 2022, ApJL, 933, L23
Mao, S., & Paczynski, B. 1991, ApJL, 374, L37
Marchant, P., Renzo, M., Farmer, R., et al. 2019, ApJ, 882, 36
Mashian, N., & Loeb, A. 2017, MNRAS, 470, 2611
Massevitch, A., & Yungelson, L. 1975, MmSAI, 46, 217
Moe, M., & Di Stefano, R. 2017, ApJS, 230, 15
Mróz, P., Udalski, A., & Gould, A. 2022, ApJL, 937, L24
Neijssel, C. J., Vigna-Gómez, A., Stevenson, S., et al. 2019, MNRAS, 490, 3740
Nomoto, K. 1984, ApJ, 277, 791
Olejak, A., Belczynski, K., Bulik, T., & Sobolewska, M. 2020, A&A, 638, A94
Paczynski, B. 1986, ApJ, 304, 1
Paczynski, B. 1996, ARA&A, 34, 419
Peters, P. C. 1964, PhRv, 136, 1224
Pfahl, E., Rappaport, S., & Podsiadlowski, P. 2002, ApJ, 573, 283
Podsiadlowski, P., Langer, N., Poelarends, A. J. T., et al. 2004, ApJ, 612, 1044
Reig, P. 2011, Ap&SS, 332, 1
Renzo, M., Zapartas, E., de Mink, S. E., et al. 2019, A&A, 624, A66
Riley, J., Agrawal, P., Barrett, J. W., et al. 2022, ApJS, 258, 34
Sahu, K. C., Anderson, J., Casertano, S., et al. 2022, ApJ, 933, 83
Salpeter, E. E. 1955, ApJ, 121, 161
Sana, H., de Mink, S. E., de Koter, A., et al. 2012, Sci, 337, 444
Seabroke, G. M., & Gilmore, G. 2007, MNRAS, 380, 1348
Shapiro, S. L., & Teukolsky, S. A. 1983, Black Holes, White Dwarfs, and Neutron Stars: The Physics of Compact Objects (New York: Wiley)
Smith, N. 2014, ARA&A, 52, 487
Soberman, G. E., Phinney, E. S., & van den Heuvel, E. P. J. 1997, A&A, 327, 620
Spergel, D., Gehrels, N., Baltay, C., et al. 2015, arXiv:1503.03757
Stevenson, S., Sampson, M., Powell, J., et al. 2019, ApJ, 882, 121
Szécsi, D., Langer, N., Yoon, S.-C., et al. 2015, A&A, 581, A15
Tauris, T. M., Kramer, M., Freire, P. C. C., et al. 2017, ApJ, 846, 170
Tauris, T. M., Langer, N., & Podsiadlowski, P. 2015, MNRAS, 451, 2123
Tauris, T. M., & van den Heuvel, E. P. J. 2006, Compact stellar X-ray sources, Vol. 39 (Cambridge: Cambridge Univ. Press), 623
Thompson, T. A., Kochanek, C. S., Stanek, K. Z., et al. 2019, Sci, 366, 637
Timmes, F. X., Woosley, S. E., & Weaver, T. A. 1996, ApJ, 457, 834
Vigna-Gómez, A., Neijssel, C. J., Stevenson, S., et al. 2018, MNRAS, 481, 4009
Vigna-Gómez, A., Schrøder, S. L., Ramirez-Ruiz, E., et al. 2021, ApJL, 920, L17
Vigna-Gómez, A., Wassink, M., Klencki, J., et al. 2022, MNRAS, 511, 2326
Vinciguerra, S., Neijssel, C. J., Vigna-Gómez, A., et al. 2020, MNRAS, 498, 4705
Vink, J. S., & de Koter, A. 2005, A&A, 442, 587
Vink, J. S., de Koter, A., & Lamers, H. J. G. L. M. 2000, A&A, 362, 295
Vink, J. S., de Koter, A., & Lamers, H. J. G. L. M. 2001, A&A, 369, 574
Webbink, R. F. 1984, ApJ, 277, 355
Wiktorowicz, G., Lu, Y., Wyrzykowski, Ł, et al. 2020, ApJ, 905, 134
Wiktorowicz, G., Wyrzykowski, Ł, Chruslinska, M., et al. 2019, ApJ, 885, 1
Willcox, R., Mandel, I., Thrane, E., et al. 2021, ApJL, 920, L37
Woosley, S. E. 2017, ApJ, 836, 244
Wyrzykowski, Ł., & Mandel, I. 2020, A&A, 636, A20
Wyrzykowski, Ł., Kostrzewa-Rutkowska, Z., Skowron, J., et al. 2016, MNRAS, 458, 3012
Xu, X.-J., & Li, X.-D. 2010a, ApJ, 716, 114
Xu, X.-J., & Li, X.-D. 2010b, ApJ, 722, 1985
Yamaguchi, M. S., Kawanaka, N., Bulik, T., & Piran, T. 2018, ApJ, 861, 21
Zapartas, E., de Mink, S. E., Justham, S., et al. 2021, A&A, 645, A6